Sulfane Sulfur Posttranslationally Modifies the Global Regulator AdpA to Influence Actinorhodin Production and Morphological Differentiation of *Streptomyces coelicolor*

Ting Lu,[a] Xiaohua Wu,[a] Qun Cao,[a] Yongzhen Xia,[a] (ORCID) Luying Xun,[a,b] (ORCID) Huaiwei Liu[a]

[a]State Key Laboratory of Microbial Technology, Shandong University, Qingdao, People's Republic of China
[b]School of Molecular Biosciences, Washington State University, Pullman, Washington, USA

ABSTRACT The transcription factor AdpA is a key regulator controlling both secondary metabolism and morphological differentiation in *Streptomyces*. Due to its critical functions, its expression undergoes multilevel regulations at transcriptional, posttranscriptional, and translational levels, yet no posttranslational regulation has been reported. Sulfane sulfur, such as hydro polysulfide (HS_nH, $n \geq 2$) and organic polysulfide (RS_nH, $n \geq 2$), is common inside microorganisms, but its physiological functions are largely unclear. Here, we discovered that sulfane sulfur posttranslationally modifies AdpA in *Streptomyces coelicolor* via specifically reacting with Cys^{62} of AdpA to form a persulfide (Cys^{62}-SSH). This modification decreases the affinity of AdpA to its self-promoter P_{adpA}, allowing increased expression of *adpA*, further promoting the expression of its target genes *actII-4* and *wblA*. ActII-4 activates actinorhodin biosynthesis, and WblA regulates morphological development. Bioinformatics analyses indicated that AdpA-Cys^{62} is highly conserved in *Streptomyces*, suggesting the prevalence of such modification in this genus. Thus, our study unveils a new type of regulation on the AdpA activity and sheds a light on how sulfane sulfur stimulates the production of antibiotics in *Streptomyces*.

IMPORTANCE *Streptomyces* species produce a myriad of natural products with (potential) clinical applications. While the database of biosynthetic gene clusters is quickly expanding, their regulation mechanisms are rarely known. Sulfane sulfur species are commonly present in microorganisms with unclear functions. Here, we discovered that sulfane sulfur increases actinorhodin (ACT) production in *S. coelicolor*. The underlying mechanism is that sulfane sulfur specifically reacts with AdpA, a global transcription factor controlling both ACT gene cluster and morphological differentiation-related genes, to form sulfhydrated AdpA. This modification changes the dynamics of AdpA-controlled gene networks and leads to high expression of ACT biosynthetic genes. Given the wide prevalence of AdpA and sulfane sulfur in *Streptomyces*, this mechanism may represent a common regulating pattern of all AdpA-controlled biosynthetic pathways. Thus, this finding provides a new strategy for mining and activating valuable biosynthetic gene clusters.

KEYWORDS sulfane sulfur, AdpA, polyketides, actinorhodin, *Streptomyces*

Streptomyces spp. are Gram-positive bacteria with a filamentous form which colonize a wide range of terrestrial and aquatic niches. The most famous characteristic of *Streptomyces* is the ability to produce a myriad of secondary metabolites, including antibiotics, antifungals, antivirals, anthelmintic agents, antitumoral drugs, antihypertensives, herbicides, and valuable pigments (1–3). Much effort has been spent on searching, identifying, and modifying the gene clusters responsible for biosynthesis of these secondary metabolites (4). In contrast, much less energy has been invested in

illustrating the transcriptional/translational regulation of these gene clusters. One reason is that *Streptomyces* have a complex life cycle that includes sporulation, a vegetative or substrate state, and aerial mycelial growth. The biosynthesis of secondary metabolites is closely linked to the stages of the life cycle (5, 6), which makes relative studies challenging.

AdpA is a transcriptional regulator universally present in *Streptomyces* (7). It is located in the second layer of the A-factor-dependent transcriptional network in *Streptomyces griseus*; the first layer is the A-factor receptor, which activates AdpA expression at the presence of A-factor (γ-butyrolactone, a quorum sensing hormone). Therefore, AdpA expression is indirectly controlled by the quorum sensing signal. Aside from A-factor, there are at least four other players in AdpA expression regulation—the master developmental regulator BldD regulating at the transcriptional level (8, 9), the *cis*-antisense RNA regulating at the posttranscriptional level (10), the rare tRNA (tRNA$^{UUA}_{Leu}$)-encoding gene *bldA*, and the posttranscriptional tRNA modifications regulating at the translational level (11, 12). It was also reported that AdpA can be transcriptionally self-inhibited (13). One reason why regulation of AdpA expression is so complicated is that AdpA is a key regulator of both secondary metabolism and morphological differentiation (14). Considering the critical functions it conducts, whether there are other players regulating at different levels on AdpA expression or activity is unclear but worthy of further investigation.

Sulfane sulfur-containing compounds, such as persulfide (HSSH and RSSH) and polysulfide (HSS$_n$H, S$_n$, RSS$_n$H, RSS$_n$R, $n \geq 2$), are commonly present in both eukaryotic and prokaryotic cells (15). In the past 2 decades, intensive studies of sulfane sulfur have been performed with mammalian cells because it was found that sulfane sulfur is involved in the regulation of diverse physiological and pathological processes, including apoptosis, carcinogenesis, and redox maintenance (16–19). On the other hand, studies of microorganism sulfane sulfur are traditionally focused on its metabolism and its role in the global sulfur cycle (20, 21). In recent years, the physiological functions of sulfane sulfur in microorganisms also got attentions. For instance, Peng et al. (22) found that sulfane sulfur regulates the expression of virulence factors in *Staphylococcus aureus*, and Liu et al. (23) reported that sulfane sulfur is involved in photosynthesis regulation in *Synechococcus*. Although they have been noticed, the functions of sulfane sulfur in microorganisms are largely obscure.

In a previous study, we discovered that sulfane sulfur functions as a signal to activate actinorhodin (ACT) production in *S. coelicolor* M145, a model strain of *Streptomyces*. In addition, the spore formation process is accelerated by endogenously accumulated sulfane sulfur (24). These phenomena suggest that sulfane sulfur affects both secondary metabolism and the cell cycle in *S. coelicolor* M145. Based on these findings, we studied the underlying mechanism of how sulfane sulfur performs such functions. We found that AdpA is the key medium of sulfane sulfur signaling. AdpA senses the level of intracellular sulfane sulfur and adjusts ACT production and spore formation. Even the expression of AdpA itself is affected by sulfane sulfur; i.e., sulfane sulfur is a new regulator of AdpA. Thus, this study unveils one way via which sulfane sulfur signals in *Streptomyces*.

RESULTS

AdpA is a key regulator of ACT production and morphological development in *S. coelicolor*. Previous studies demonstrated that AdpA is involved in the regulation of ACT production and morphological development in *S. coelicolor* (25, 26). Here, we constructed an *adpA*-disrupted *S. coelicolor* M145 strain ($\Delta adpA$). It exhibited a phenotype of no ACT but high undecylprodigiosin (RED) production when cultured on yeast-beef-peptone (YBP) agar medium (Fig. 1A). Complementary expression of the *adpA* gene using a plasmid, pMS82-*adpA* ($\Delta adpA$::*adpA*), restored ACT production, while the control, $\Delta adpA$ harboring an empty plasmid ($\Delta adpA$::pMS82), showed no change. In addition, we noticed that both $\Delta adpA$ and the control showed a bald and nonspore form on YBP medium (Fig. 1A), while $\Delta adpA$::*adpA* restored the spore formation. These
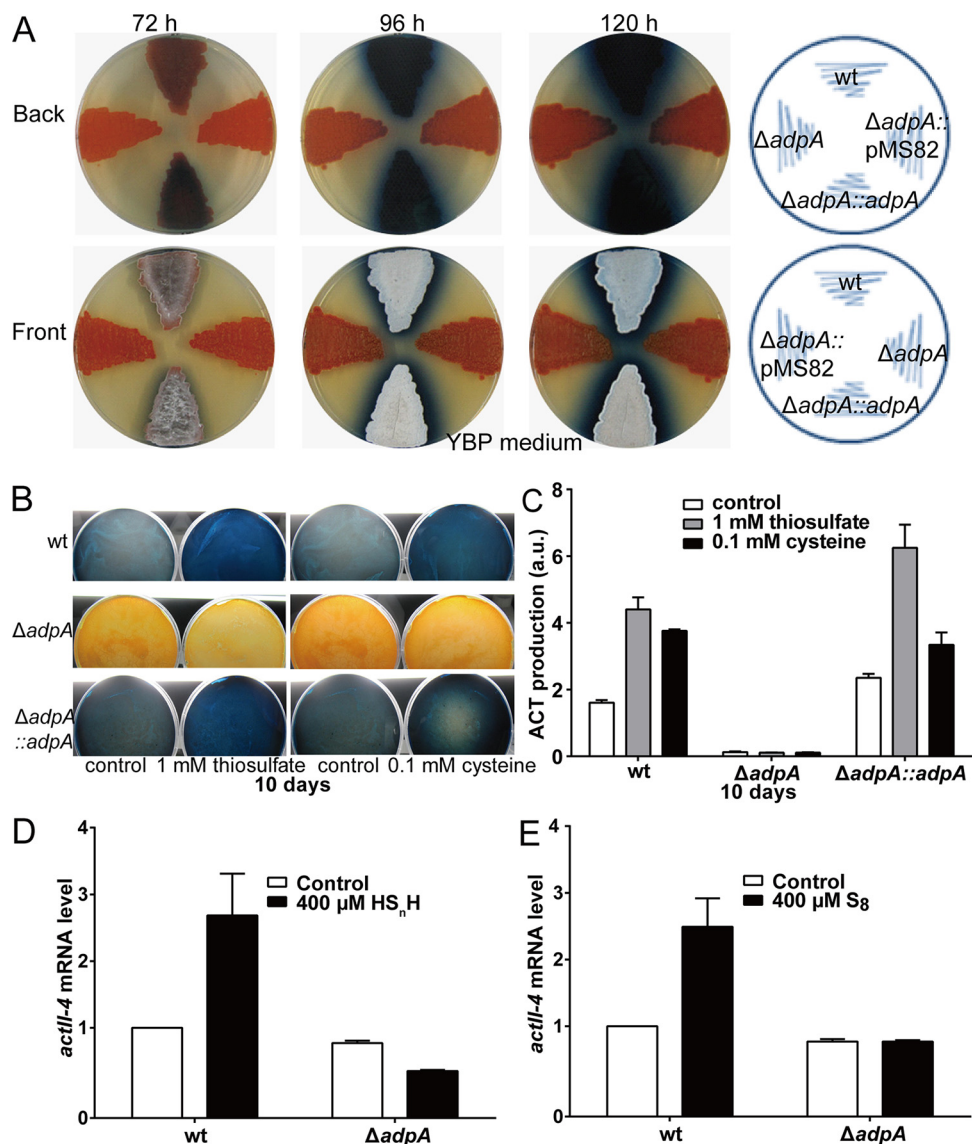
FIG 1 AdpA is required for ACT production and morphological development in *S. coelicolor* M145. (A) Phenotypes of the WT, Δ*adpA*, Δ*adpA::adpA*, and Δ*adpA*::pMS82 strains grown on YBP medium at 30°C. Images were taken at the indicated times. (B) First, 1 mM thiosulfate or 0.1 mM cysteine was added to YBP agar plates before inoculation. The plates were incubated at 30°C for 10 days, and images were captured from the reverse side of the plates. (C) Quantitative determination of ACT produced by the wt, Δ*adpA*, and Δ*adpA::adpA* strains on YBP containing thiosulfate or cysteine. The plates were incubated at 30°C for 10 days. Data are from three independent repeats. (D and E) WT and Δ*adpA* strains were grown on YBP liquid medium. At 36 h, 400 μM HS_nH or S_8 was added, and after 1 h of induction, RNA samples were isolated. Real-time PCR data are from three independent repeats and shown as the average $\pm$ standard deviation (SD).

results verified that AdpA controls ACT production and morphological development in *S. coelicolor* strain M145.

Sulfane sulfur performing ACT activation requires the presence of AdpA. Since the Δ*adpA* strain displayed opposite phenotypes as that of the sulfane sulfur-treated strain (24), we suspected that AdpA had interwound functions with sulfane sulfur. We performed sulfane sulfur induction experiments using the *S. coelicolor* M145 (wild type [WT]), Δ*adpA*, and Δ*adpA::adpA* strains. The strains were spread on YBP medium containing 1 mM thiosulfate or 0.1 mM cysteine, which can be converted to sulfane sulfur *in vivo* (27), and cultured at 30°C for 10 days. For the WT, the production of ACT was significantly increased by thiosulfate/cysteine treatment (Fig. 1B and C). For Δ*adpA*, no
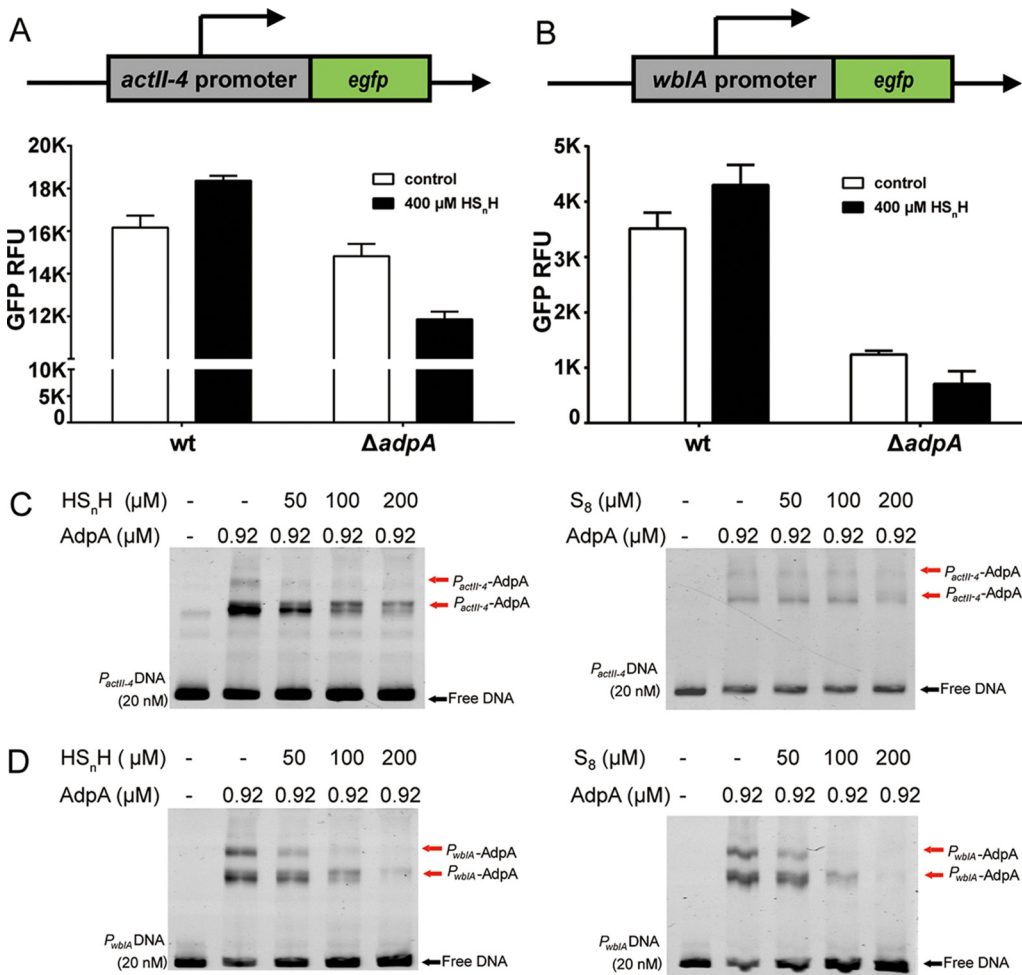
FIG 2 Sulfane sulfur is involved in the process of AdpA regulating target genes. (A) HS$_n$H was used to treat WT and $\Delta adpA$ strains harboring pMS82-*actII-4*p-*egfp*. (B) HS$_n$H was used to treat WT and $\Delta adpA$ strains harboring pMS82-*wblA*p-*egfp*. Data are from three independent repeats and shown as the average $\pm$ SD. (C and D) EMSA analysis of the AdpA affinity to P$_{actII-4}$ promoter DNA (C) and the P$_{wblA}$ promoter DNA (D). All lanes contained 20 nM probe DNA, lanes 2 to 5 contained protein with the indicated concentration, and lanes 3 to 5 contained the HS$_n$H (left) or S$_8$ (right). The black arrow indicates the free DNA probe, and red arrows indicate the P$_{actII-4}$-AdpA or P$_{wblA}$-AdpA complex.

production of ACT was observed with or without thiosulfate/cysteine treatment. For $\Delta adpA$::*adpA*, the induction effects were similar to those in the WT (Fig. 1B and C). These results indicated that AdpA is required for sulfane sulfur to execute the ACT production-activating function.

ActII-4 is the ACT production "pathway-specific" activator (26, 28). We analyzed transcription of *actII-4* using the real-time quantitative reverse transcription-PCR (RT-qPCR) method. The WT and $\Delta adpA$ strains were treated with two sulfane sulfur-containing chemicals, hydrogen polysulfides (HS$_n$H, $n \geq 2$) and sublimed sulfur (S$_8$). For the WT, the transcription level of *actII-4* was much higher in the treated strain than that in the untreated one (Fig. 1D and E), whereas for $\Delta adpA$, the transcription level of *actII-4* had no obvious change after sulfane sulfur treatment (Fig. 1D and E). These results indicated that sulfane sulfur can increase ActII-4 expression, which subsequently activates ACT production, but this process requires the presence of AdpA.

Sulfane sulfur affects the interaction between AdpA and its cognate promoters. AdpA controls the transcription of *actII-4* and *wblA* (*whiB*-like gene A, which controls morphological development in *S. coelicolor*) via binding to their promoters (29). Using these two promoters and an enhanced green fluorescence protein-encoding gene (*egfp*), we constructed two reporter systems (Fig. 2A and B). These reporter systems
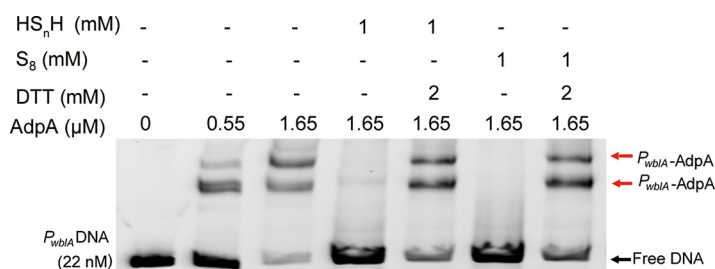
FIG 3 EMSA analysis of AdpA binding to P_{wblA} promoter DNA. All lanes contained 22 nM P_{wblA} DNA, lanes 2 to 7 contained AdpA, lanes 4 and 5 contained HS_nH, lanes 6 and 7 contained S_8, lanes 5 and 7 contained DTT.

were introduced into the WT and $\Delta adpA$ strains. HS_nH (400 μM) was used to treat the strains containing the reporter systems. After 30 min of treatment, the mycelium was collected by centrifugation, and the fluorescence was read by a fluorophotometer. For the WT strain, HS_nH treatment enhanced the strength of both the *actII-4* promoter ($P_{actII-4}$) and *wblA* promoter (P_{wblA}), evidenced by the increased EGFP expression, whereas, in the $\Delta adpA$ strain, EGFP expression was not increased but decreased after HS_nH treatment, indicating that HS_nH treatment lost the enhancing effect on these promoters. These results suggested that sulfane sulfur may affect the interaction between AdpA and its cognate promoters.

We then performed electrophoretic mobility shift assays (EMSA) to investigate the interaction. The AdpA protein was expressed in *Escherichia coli* BL21(DE3) and purified. The DNA probes of the *wblA* and *actII-4* promoters were obtained by PCR. When AdpA was mixed with the $P_{actII-4}$ or P_{wblA} DNA probe, it bound to them (Fig. 2C and D). When HS_nH (200 μM) or S_8 (200 μM) was also added, the fraction of the AdpA-probe complexes decreased (Fig. 2C and D). These results indicated that sulfane sulfur decreased the affinity of AdpA to $P_{actII-4}$ and P_{wblA}.

To test whether the influence of sulfane sulfur can be reversed by a reductant, we added dithiothreitol (DTT) into the mixture of sulfane sulfur (1 mM), AdpA, and the P_{wblA} probe (the DTT dosage was 2-fold of HS_nH/S_8). After DTT treatment, AdpA restored the high affinity with the P_{wblA} probe (Fig. 3), which had been attenuated by sulfane sulfur. These phenomena demonstrated that the affinity attenuation of AdpA to its cognate DNA caused by sulfane sulfur was reversible.

Sulfane sulfur also affects the transcription of AdpA itself. The *adpA* gene is transcriptionally self-controlled (30). There are five AdpA binding sites in the P_{adpA} promoter (Fig. 4A). We designed a pair of primers (*adpA-wt*) from the undeleted part of the *adpA* gene (Fig. 4B) and used these primers to analyze the transcription change of *adpA* in the WT and $\Delta adpA$. The transcription level of the undeleted part was ~30-fold higher in $\Delta adpA$ than that in the WT, indicating that in the absence of AdpA, the strength of P_{adpA} was higher, i.e., AdpA acted as a repressor for its own transcription (Fig. 4C).

To test whether sulfane sulfur can affect this self-repression, we compared the transcription levels of *adpA* in the WT stain and the Δpdo strain. In the latter, intracellular sulfane sulfur is accumulated due to a lack of the persulfide oxidation gene (*pdo*) (24). Results showed that the *adpA* transcription levels were higher in Δpdo than in the WT (Fig. 4D). We then used exogenous sulfane sulfur to treat the WT strain and found that both HS_nH (400 μM) and S_8 (400 μM) can increase *adpA* transcription (Fig. 4E and F). EMSA showed that sulfane sulfur (100 to 200 μM) also reduced the affinity of AdpA to P_{adpA} probe, as the unbound probe increased after the addition of HS_nH and S_8 (Fig. 5A). Fluorescence polarization (FP) analysis was performed, and the results showed that HS_nH (500 μM) obviously increased the K_D value (the equilibrium dissociation constant) of AdpA to the P_{adpA} probe, as well as to the P_{wblA} probe (Fig. 5B and C), indicating that the affinities of AdpA to these promoters were attenuated by HS_nH.
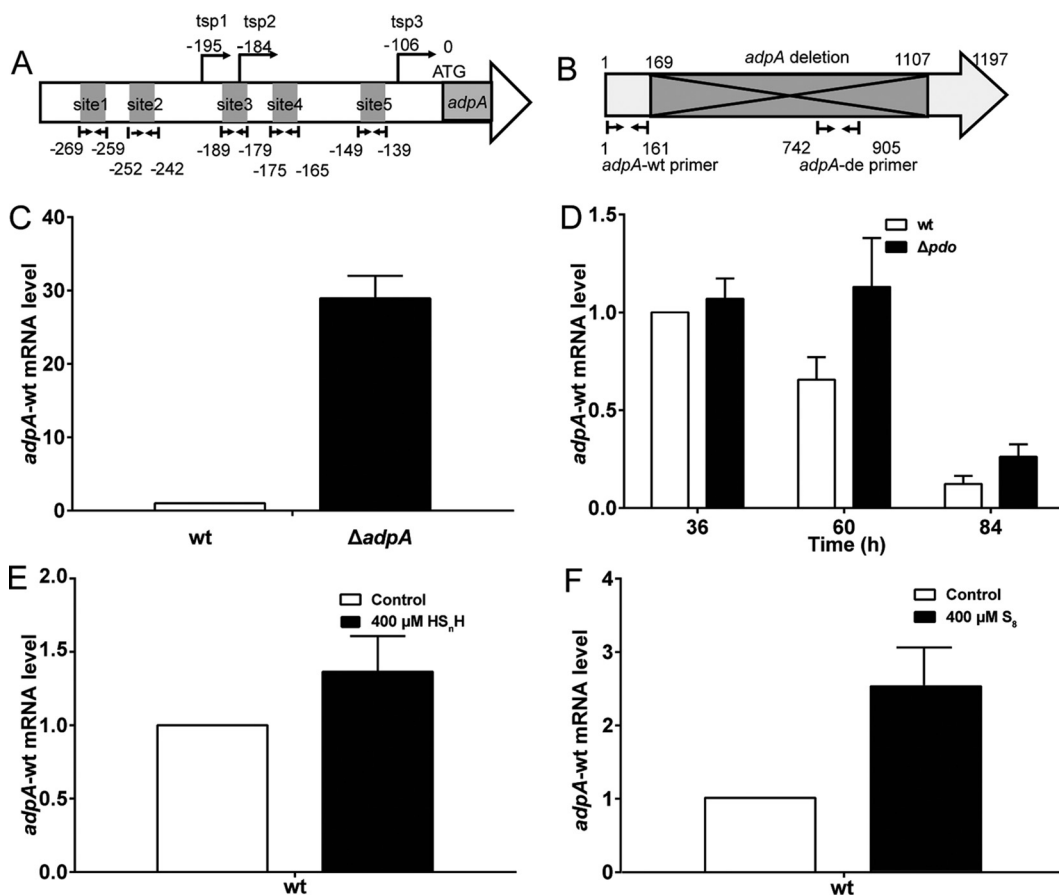
FIG 4 Sulfane sulfur affects the transcription of *adpA* itself. (A) Schematic diagram of the AdpA binding sites in the *adpA* promoter region. (B) Schematic diagram of the AdpA coding sequence. The fragment covering 169 bp to 1,107 bp was deleted in Δ*adpA*. The *adpA*-wt and *adpA*-de primers were used to test the undeleted and deleted sequences, respectively. (C) RT-qPCR analysis of the *adpA*-wt mRNA level in the WT and Δ*adpA*. (D) RT-qPCR analysis of *adpA*-wt mRNA level in the WT and Δ*pdo*. Data are from three independent repeats and shown as the average ± SD. (E and F) RT-qPCR analysis of *adpA*-wt in the WT and Δ*adpA* after induction by HS$_n$H (400 μM) (E) and S$_8$ (400 μM) (F). Data are from three independent repeats and shown as the average ± SD.

Simulating the dynamics of the AdpA-controlled promoter system with a simplified model. For the regulation of AdpA on P_{adpA} strength, the logic is easy to understand; P_{adpA} and AdpA compose a classic closed negative-feedback loop. AdpA is a repressor of P_{adpA}. When AdpA is abundant, it binds with P_{adpA} to turn it off/down. The off/down state lasts until the AdpA concentration becomes low due to degradation, and then P_{adpA} turns on/up again. Therefore, without other interference, the strength of P_{adpA} fluctuates, leading to a wave-like expression pattern of AdpA. Since AdpA is an activator of P_{act-4}, the expression of Act-4 also fluctuates following the concentration wave of AdpA. The principle of these dynamics can be simulated with a simplified mathematical model (Fig. 6A).

For the regulation of AdpA on P_{actII} and P_{wblA}, there is a paradoxical phenomenon; reporter system and RT-qPCR experiments indicated that AdpA enhanced the strength of these two promoters in the presence of sulfane sulfur, but EMSA and FP experiments indicated that sulfane sulfur decreased the AdpA affinities to them. There are several possible reasons for this paradox:

1. There is another player, possibly a transcription factor (TF), involved in this system. This unknown TF takes the place of AdpA in the presence of sulfane sulfur and then further increases P_{actII}/P_{wblA} strength.

2. Sulfane sulfur leads to increased AdpA production, and when the concentration of AdpA is higher than that of sulfane sulfur, free AdpA is more abundant than
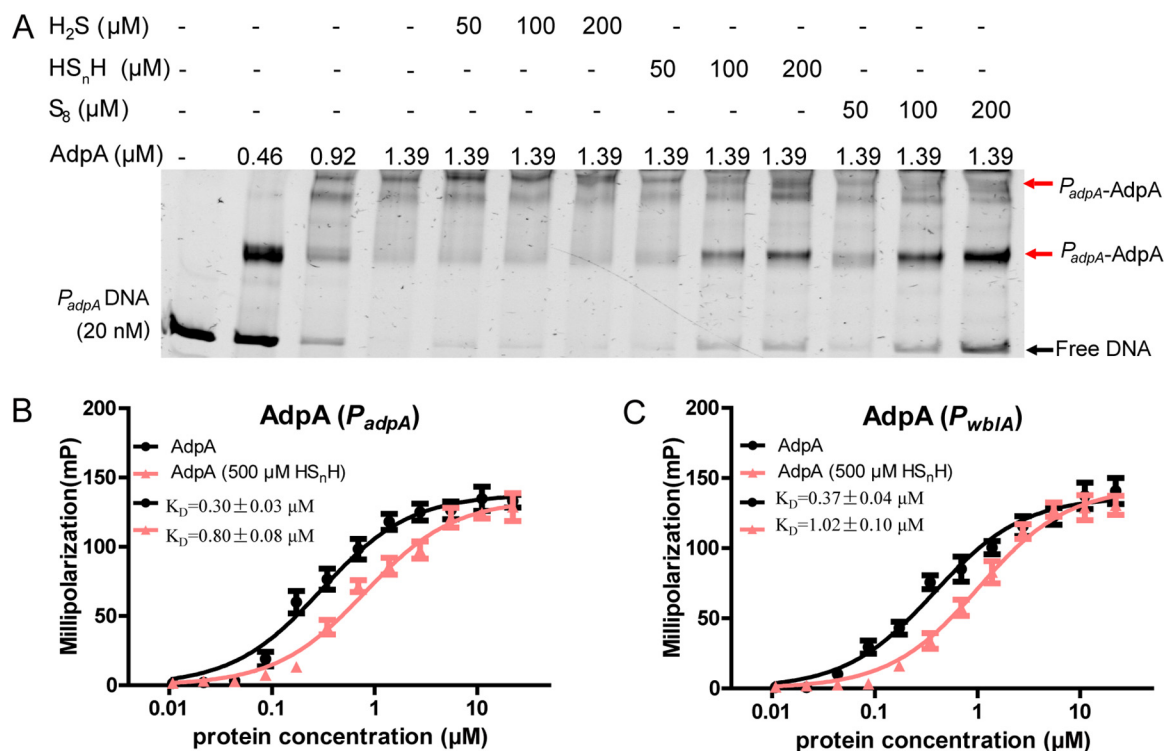
FIG 5 EMSA and FP analysis of AdpA binding to DNA probes. (A) EMSA analysis of AdpA binding to the P_{adpA} probe. All lanes contained 20 nM probe, lanes 2 to 13 contained AdpA, lanes 5 to 7 contained H_2S (50, 100, and 200 μM, respectively), lanes 8 to 10 contained HS_nH (50, 100, and 200 μM, respectively), and lanes 11 to 13 contained S_8 (50, 100, and 200 μM, respectively). (B and C) FP analysis of AdpA binding to the P_{adpA} probe (B) and P_{wblA} probe (C). First, 1 nM FAM-labeled P_{adpA} or P_{wblA} was incubated with increasing amounts of AdpA or HS_nH (500 μM)-treated AdpA. The K_D values were calculated based on FP data using GraphPad Prism 5 software. Data are from three independent experiments and shown as the average $\pm$ SD.

the sulfane sulfur-modified AdpA. In this case, free AdpA binds to P_{actII}/P_{wblA} and enhances their strength.

3. The affinities of sulfane sulfur-modified AdpA to P_{adpA}, P_{actII}, and P_{wblA} are different. These differences lead to variations in the transcriptional levels of these genes.

Previously, we observed that the concentration of intracellular sulfane sulfur of *S. coelicolor* changed along with expression levels of its metabolic genes (24). Therefore, it is highly possible that the ratio of sulfane sulfur to AdpA (S⁰/AdpA) is dynamic (a scenario in item 2). To understand how S⁰/AdpA influences the strength of $P_{actII-4}$ and P_{adpA}, we developed another mathematical model; at the initial stage, S⁰/AdpA is high, so the sulfane sulfur-reacted AdpA (AdpA-S) is the dominant form (more abundant than *apo* AdpA), which leads to enhanced expression of *adpA* but not *actII-4* (Fig. 6B). Before S⁰ is completely consumed, AdpA is continuously produced, leading to a higher level of AdpA than that in the wave-like expression pattern. However, along with consumption of S⁰, S⁰/AdpA gradually reduces, and finally *apo* AdpA becomes the dominant form; then the AdpA system returns to its closed negative-feedback loop as shown in Fig. 6A. Based on this simulation, we proposed that sulfane sulfur can temporarily break the self-inhibition in AdpA expression, allowing AdpA to accumulate to a higher level for a longer period (compared with the no-sulfane sulfur scenario), which finally leads to more ActII-4 expression.

The cysteine residue Cys⁶² is critical for AdpA sensing sulfane sulfur. Sulfane sulfur can react with cysteine residues of certain proteins to change their configurations (31, 32). AdpA contains four cysteine residues, Cys⁶², Cys¹²⁶, Cys¹⁸⁷, and Cys³⁰⁷. To find out which cysteine residue involves in the AdpA-sulfane sulfur interaction, we made a cysteine-to-serine mutation on each cysteine residue of AdpA. The mutated *adpA* genes were introduced into the Δ*adpA* strain. When growing in YBP agar medium, the
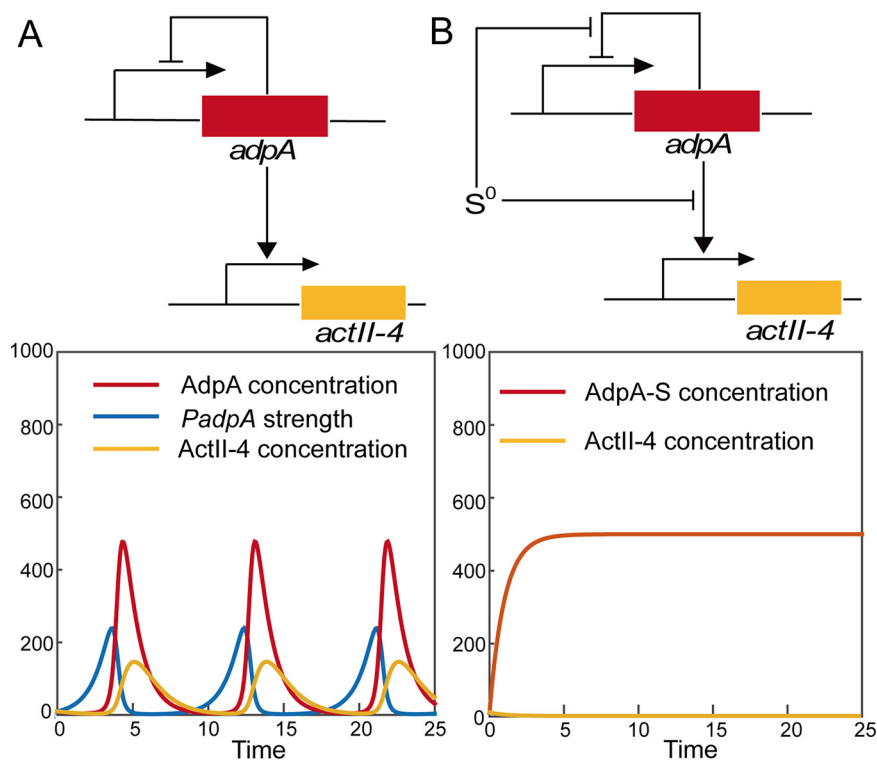
FIG 6 Modeling principles of how AdpA regulates *adpA* and *actII-4* expression. (A) In the absence of sulfane sulfur, P_{adpA} is self-repressed by AdpA to form a negative-feedback loop, and hence, both P_{adpA} strength and AdpA amount show a wave-like pattern. (B) Sulfane sulfur temporarily breaks the negative-feedback loop, which leads to a higher and longer expression of AdpA but not ActII-4 at the initial stage. After sulfane sulfur is consumed, the high AdpA level will lead to high expression of ActII-4. Equations and related parameters used for modeling are provided in Text S1.

$\Delta adpA::adpA_{C126S}$, $\Delta adpA::adpA_{C187S}$, and $\Delta adpA::adpA_{C307S}$ strains did not show obvious difference from the WT and $\Delta adpA::adpA$ strains. However, the $\Delta adpA::adpA_{C62S}$ strain was distinct from the others. It lost the ability to generate spores, and its ACT production was also apparently lower (Fig. 7A). These phenotype changes indicated that Cys[62] was critical for AdpA performing its regulatory function.

EMSA was then performed to examine whether the C62S mutation affects the binding of AdpA to its cognate promoter. AdpA$_{C62S}$ still bound to the P_{wblA} DNA fragment, and two main P_{wblA}-AdpA$_{C62S}$ complexes with different molecular weights (MW) were observed. The complex with lower MW was no longer influenced by sulfane sulfur even when sulfane sulfur was added at high concentrations (>1,000-fold higher than that of AdpA$_{C62S}$) (Fig. 7B), whereas the complex with higher MW disappeared when high concentrations of sulfane sulfur were added. Since the lower-MW complex was the most abundant one formed by AdpA$_{C62S}$ and the P_{wblA} DNA fragment, we proposed that the sulfane sulfur sensing ability was at least partially impaired by the C62S mutation.

To check how sulfane sulfur reacts with AdpA, purified AdpA was treated with HS_nH (200 μM) or DTT (200 μM). The treated-AdpA was labeled with iodoacetamide (IAM) and then subjected to trypsin digestion, followed by LTQ-Orbitrap tandem mass spectrometry analysis. For the HS_nH-treated AdpA, two peptides (1 and 2, Fig. 8) were identified. In peptide 1 (1,299.67 Da), the Cys[62] residue was directly blocked by IAM to form Cys[62]-AM (acetamide) (Fig. 8 and Fig. S1). In peptide 2 (1,331.64 Da), a mass increase of 32 (+32 MW) was identified. A secondary mass spectrometry(MS[2]) spectrum indicated that the +32 MW happened on the thiol group of Cys[62] to form peptide-S-AM (Fig. 8 and Fig. S2). The MS[1] signal intensity ratio of peptide 1/peptide 2 was 17%. As the control, only a peptide with Cys[62]-AM (1,299.67 Da, peptide 3) was identified from DTT-reacted AdpA, corresponding to a direct blockage of IAM on the Cys[62] residue (Fig. 8
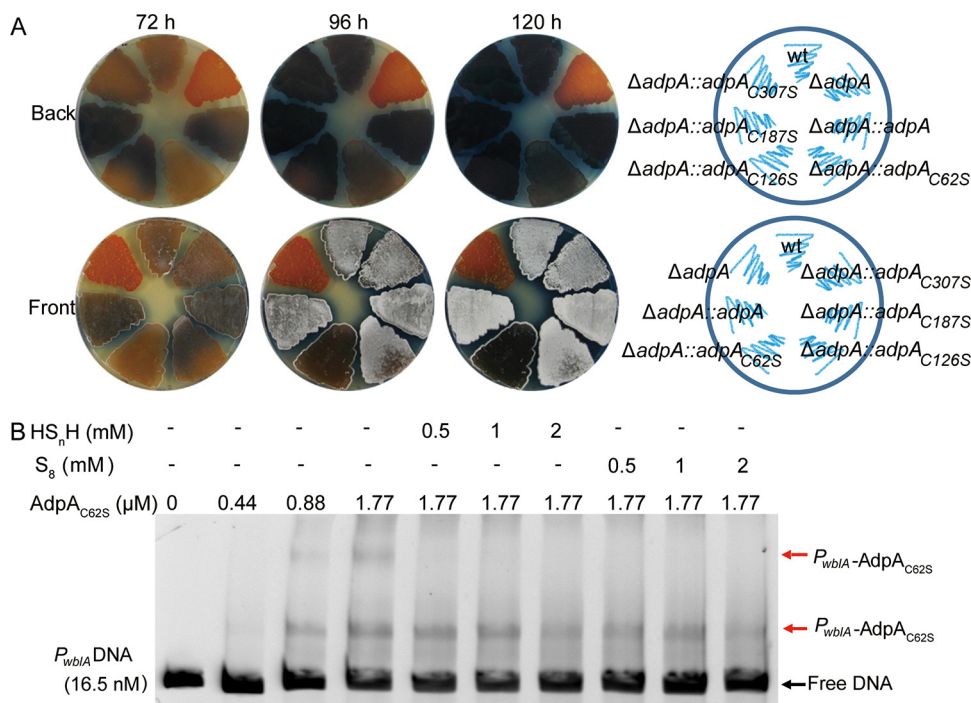
FIG 7 Cys[62] residue is critical for AdpA sensing sulfane sulfur. (A) Phenotypes of WT, $\Delta adpA$, and complementary strains ($\Delta adpA::adpA_{C62S}$, $\Delta adpA::adpA_{C126S}$, $\Delta adpA::adpA_{C187S}$, and $\Delta adpA::adpA_{C307S}$) grown on YBP medium. Images were captured from both sides of the plates. (B) EMSA analysis of AdpA$_{C62S}$ binding to P_{wblA} DNA. All lanes contained 16.5 nM probe DNA, lanes 2 to 10 contained AdpA, lanes 5 to 7 contained HS$_n$H, and lanes 8 to 10 contained S$_8$. The black arrow indicates the free DNA probe, and red arrows indicate the P_{wblA}–AdpA$_{C62S}$ complex.

and Fig. S3). These results indicated that sulfane sulfur can modify Cys[62]-SH to form Cys[62]-SSH.

The thiol group of Cys62 is accessible to solution due to its location on the AdpA 3D structure. The 3D structure of AdpA was modeled by using AlphaFold 2 (https://www.hpc.caltech.edu/documentation/software-and-modules/alphafold-2). The crystal structure of a truncated AdpAsg containing only the DNA binding domain, which is from *Streptomyces griseus*, is available in the PDB database (PDB: 3w6v). We aligned AdpAsg with the modeled AdpA, and the alignment parameter RMSD was 0.365, indicating a high confidence of the predicted structure of AdpA (Fig. 9A and B).

We then analyzed the locations of the four cysteine residues in AdpA (Fig. 9C). Cys[62], Cys[126], and Cys[187] are located in the ThiJ/PfpI/DJ-1-like dimerization domain, and Cys[307] is located in the AraC/XylS-type DNA binding domain (DBD). Cys[187] and Cys[307]
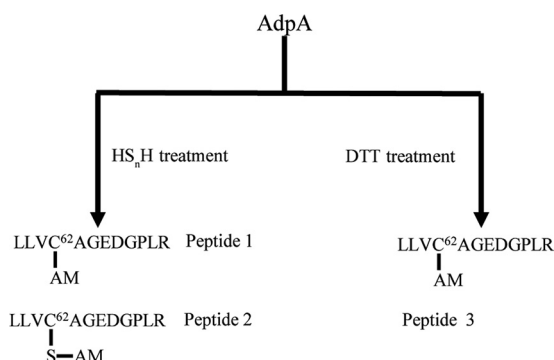

FIG 8 LC-MS/MS analysis of HS$_n$H-treated and DTT-treated AdpA. MS^2 data of the peptides are provided in Fig. S1 to S3.
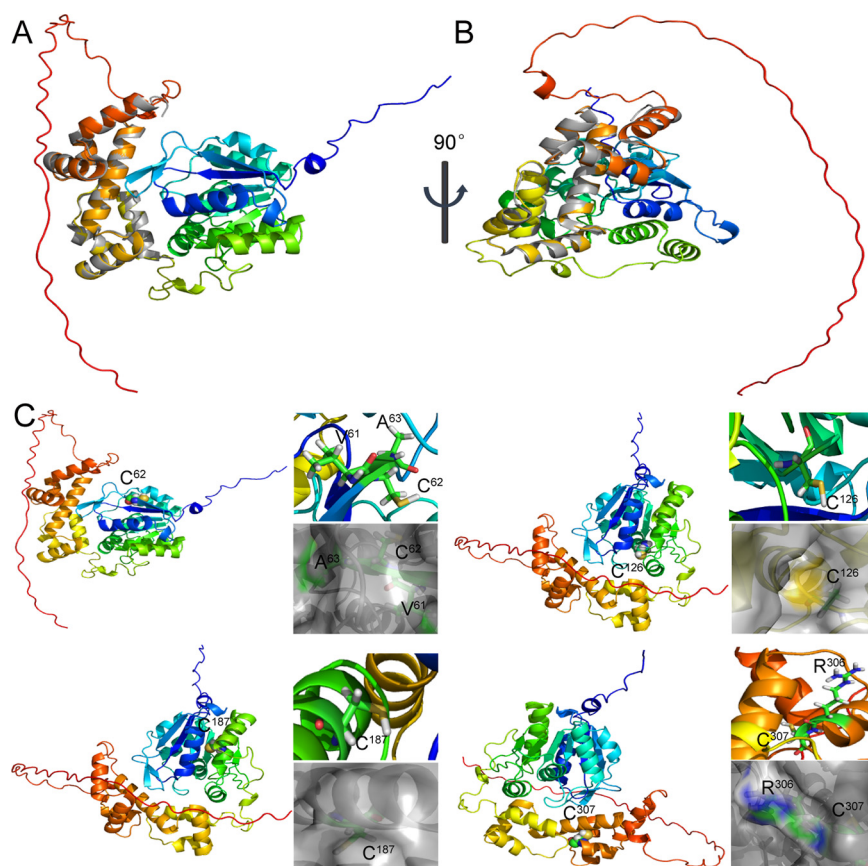
FIG 9 AlphaFold 2-predicted 3D structure of AdpA. (A and B) Alignment of the predicted AdpA structure (multicolor) with the AdpAsg crystal structure (gray). (C) Locations of the cysteine residues in AdpA. Yellow spheres represent the sulfur atoms.

fold into the interior of AdpA, and hence they are protected from sulfane sulfur attack. In contrast, Cys^{62} is located near the protein surface, and its thiol group is exposed to solution, which may explain why Cys^{62} can be modified by sulfane sulfur. It is noteworthy that Cys^{126} is located on the interior surface of a tunnel through the dimerization domain. Therefore, sulfane sulfur compounds may not enter this tunnel to react with its thiol group. In addition, the distance between any two cysteine residues is too far to form a disulfide (S-S) or tri-sulfide (S-S-S) bond.

The cysteine residues are conserved in *Streptomyces* AdpAs. We analyzed AdpA and its homologues in the *Streptomyces* genus. In the PATRIC database, 2,752 of 3,033 sequenced *Streptomyces* strains contain AdpA, accounting for a 90.73% prevalence. We selected some representative AdpA sequences to construct a phylogenetic tree. The results revealed that AdpA homologues were not on one evolutionary branch (Fig. S4). However, when we performed multiple sequence comparisons with them, we found that their four cysteine residues were highly conserved, including Cys^{62} (Fig. S5). These results suggested that using cysteine residues to sense sulfane sulfur may be a common mechanism for AdpA functioning in *Streptomyces*.

DISCUSSION

The global transcription factor AdpA plays an important role in regulation of secondary metabolism and morphological development in the *Streptomyces* genus (33–37). Its own expression is controlled by multiple factors. In this study, we discovered that sulfane sulfur affects AdpA activity via the posttranslational modification. After reacting with sulfane sulfur, the affinity of AdpA to its cognate promoters, P_{adpA}, $P_{actII-4}$, and P_{wblA}, is attenuated. We constructed a simplified model to help understand the

effect of sulfane sulfur on the AdpA-controlled promoters. As shown in our simulation (Fig. 6), P_{adpA} is under the control of a negative feedback loop of self-repression. Without the presence of sulfane sulfur and/or other disturbing factors, activation of AdpA on *actII-4* and *wblA* expression cannot last long due to the negative feedback. Sulfane sulfur modifies AdpA to temporarily break the self-repression, and hence, AdpA can accumulate to a higher level for a longer time until sulfane sulfur is consumed. The accumulated AdpA finally activates expression of *actII-4* and *wblA*. Thus, the effect of sulfane sulfur on the AdpA regulon may represent a fine-tuned regulation for the production of antibiotics and morphological development.

Furthermore, we found that Cys^{62} is critical for AdpA sensing sulfane sulfur. Our *in vitro* experiments showed that sulfane sulfur treatment can lead to a sulfhydration modification in Cys^{62} (Cys^{62}-SSH), and this modification was not observed in the other three cysteine residues of AdpA. A limitation of this work is that such modification has not been examined *in vivo* due to the lack of a trustable method. The AlphaFold 2 predicted structure shows that the thiol of Cys^{62} is accessible to solution, while the other thiols are not, which may explain why Cys^{62} is easily sulfhydrated by sulfane sulfur. However, we also noticed that AdpA and $AdpA_{C62S}$ formed different complexes with the P_{wblA} DNA fragment even in the absence of sulfane sulfur, suggesting that the binding pattern was affected by C62S mutation. Since Cys^{62} is located in the dimerization domain, it may affect the dimerization and then alter the AdpA binding pattern. Therefore, C62S mutation may result in multiple influences, including both DNA binding and sulfane sulfur sensing.

It is noteworthy that the AdpA complemented strain (Δ*adpA*::*adpA*) shows a peculiar pattern of ACT production—the center of the plate lacks the characteristic blue color—in the plates containing 0.1 M cysteine (Fig. 1B). A similar pattern was described in a recent report (38), and the authors linked the pattern formation to AdpA. Therefore, the peculiar pattern observed in our experiment may be caused by both AdpA expression alteration and cysteine addition. In the same report the authors discovered that expression of *adpA* and other genes controlled by it displayed a spatiotemporally separated wave-like pattern when *S. coelicolor* was cultured in solid medium and found that this pattern was driven by a combination of physiological gradients and regulatory network architecture (38). The finding is consistent with our simulation. From a genetic architecture viewpoint, the negative feedback loop inevitably leads to wave-like expression of *adpA*. However, the frequency (or wavelength) of the "wave" can be altered by environmental factors such as sulfane sulfur or siderophore. Understanding how the pattern forms and its determinants surely are important for interpreting the complicated differentiation process of *Streptomyces* and hence worth further study.

Streptomyces mainly exist in terrestrial soils, but they also have been detected in extreme environments such as deep seas, the north and south poles, hydrothermal fluids, hot springs, etc. In some environments (such as sea/lake bed) sulfane sulfur levels can be high, up to ~400 μM. Therefore, the possibility that *Streptomyces* live in sulfane sulfur-rich conditions cannot be excluded. In addition, sulfane sulfur has been recognized as a common intracellular chemical nowadays, and its concentration varies from 10 μM to ~500 μM (39). Hence, both self-produced and environmental sulfane sulfur may affect secondary metabolism and morphological development of *Streptomyces*.

In recent years, a few transcription factors that can be modified by sulfane sulfur have been identified from different microorganisms (40, 41). These transcription factors can be categorized into two groups. Group I consists of specific regulators for genes related to sulfur metabolism, including BigR (42), CstR (43), FisR (44), CsoR (24), and SqrR (45, 46). They control the expression of sulfane sulfur oxidation enzyme PDO and sulfane sulfur transferase RhoD (BigR in this case). Since H_2S oxidation enzyme SQR is often located in the same operon with PDO and RhoD, they also control SQR expression (CstR, FisR, and SqrR in this case) (47). Group I regulators can sense the intracellular level of sulfane sulfur via their cysteine residues; when the sulfane sulfur level is

high, cysteine residues are sulfhydrated to form an RS_nH ($n \geq 2$) or RS_nR ($n \geq 3$) bond, which leads to a configuration change of the regulator and subsequently high expression of PDO and other genes, and then the sulfane sulfur level is decreased through being oxidized to sulfite (20). Therefore, group I regulators mainly function as managers to maintain the homeostasis of intracellular sulfane sulfur.

Group II includes global or multifunctional transcription factors currently including MgrA (22), MexR (48), and OxyR (40). MgrA is a global virulence regulator of *Staphylococcus aureus*. It senses the intracellular level of sulfane sulfur to regulate the expression of virulence factors (22). MexR controls the multiple-antibiotic resistance process in *Pseudomonas aeruginosa*, and it senses intracellular sulfane sulfur to regulate the expression of the *mexAB-oprM* multidrug efflux operon (48). OxyR is a global antioxidation regulator in many bacteria. Recently, it was found that OxyR also senses sulfane sulfur and controls the expression of sulfane sulfur-reducing enzymes (40). Like group I, group II regulators also sense sulfane sulfur via their cysteine residues.

AdpA is deemed a group II regulator since it senses sulfane sulfur and accordingly adjusts the ACT production and spore formation in *S. coelicolor*. Bioinformatics analyses indicated that AdpA and its Cys residues are highly conserved in *Streptomyces* spp. Further investigation of this protein and its homologues should provide insights into how sulfane sulfur regulates the production of secondary metabolites and morphological developments in this genus. The widespread existence of AdpA implies that sulfane sulfur may play a wide range of regulatory functions in *Streptomyces*, providing unlimited possibilities for sulfane sulfur working as a signal molecule to stimulate increased production of important secondary metabolites, such as antibiotics, antitumor drugs, immunosuppressants, and antibiotics.

MATERIALS AND METHODS

Bacterial strains, plasmids, and growth conditions. All strains and plasmids used or constructed in this work are summarized in Table S1.

Streptomyces strains cultivated at 30°C on mannitol soya flour (MS) solid medium (49) or yeast-beef-peptone (YBP) solid or liquid medium (50) were used for different experiments, including spore suspension preparation, intergeneric conjugation, growth assay, RNA isolation, and phenotypic observation. All *E. coli* strains were cultured at 37°C on solid or liquid Luria-Bertani (LB) medium. The *E. coli* DH5α and *E. coli* BL21(DE3) strains were used as hosts for plasmid construction and protein expression, respectively. *E. coli* ET12567 (pUZ8002) was used as a medium for transferring nonmethylated DNA to *Streptomyces*. When required, ampicillin (100 μg/mL), apramycin (50 μg/mL), chloramphenicol (25 μg/mL), kanamycin (50 μg/mL), hygromycin (50 μg/mL), or nalidixic acid (25 μg/mL) was added into the medium.

Preparation of sulfane sulfur species and other sulfur-containing compounds. Sodium hydrosulfide (NaHS, H_2S donor), cysteine, sulfur power, and thiosulfate were purchased from Sigma-Aldrich. S_8 solution was prepared by dissolving excess sulfur powder in acetone to saturation. The concentration of saturated acetone sulfur is determined as 17 mM as reported previously (51). The stock solution of HS_nH was prepared by mixing sulfur powder, NaOH, and NaHS (40 mM each chemical) in degassed distilled water at 30°C until the powder was completely dissolved as previously described (48, 52). The concentrations of HS_nH were determined with the cyanolysis method (53) and calibrated by using thiosulfate as the standard. Specifically, pipetting 550 μL 1% boric acid into a 1.5-mL Eppendorf (EP) tube and removing dissolved oxygen by putting the EP tube in boiling water for 1 min and then adding 250 μL sample and 200 μL 1 M potassium cyanide. After boiling in a water bath (100°C) for 1 min, the EP tube was taken out and cooled down to room temperature, and 100 μL ferric nitrate color solution was added to form $Fe(SCN)_3$. The A_{460nm} absorbance value was detected. Thiosulfate was used to make a standard curve.

Construction of *S. coelicolor* ΔadpA. All primers used in this experiment are listed in Table S2. The strain Δ*adpA* was constructed using a homologous recombination method (54). Briefly, a 939-bp region was deleted from the open reading frame (ORF) of *adpA*, leaving the upstream 168 bp (relative to the start codon) and the downstream 90-bp (relative to the stop codon) coding sequence of *adpA*. The knockout region was replaced by the apramycin resistance gene. The conjugation transfer was accomplished using the methylation-sensitive strain *E. coli* ET12567/pUZ8002 (containing the mutant plasmid pJTU-*adpA*) and *S. coelicolor* M145 following a previously reported protocol (55). The deletion mutant was verified by resistance screening and colony PCR with the primers VeradpA-F/R.

Construction of Δ*adpA*::*adpA*, Δ*adpA*::pMS82, Δ*adpA*::*adpA*$_{C62S}$, Δ*adpA*::*adpA*$_{C126S}$, Δ*adpA*::*adpA*$_{C187S}$, and Δ*adpA*::*adpA*$_{C307S}$. A DNA fragment carrying the *adpA* ORF (1,197 bp) and its promoter (500 bp) was obtained using PCR amplification and was connected to the ΦBT1 integrative vector pMS82 (56) to generate pMS82-*adpA* plasmid (Table S1). This plasmid was then integrated into the *attP* site of the Δ*adpA* genome by intergeneric conjugation. To construct the negative-control strains, empty pMS82 vector was also transformed into Δ*adpA*; these derivative strains were selected and confirmed by PCR and DNA sequencing.

To construct other AdpA complementary strains, we used a point mutation strategy (57) to construct plasmids pMS82-$adpA_{C62S}$, pMS82-$adpA_{C126S}$, pMS82-$adpA_{C187S}$, and pMS82-$adpA_{C307S}$. The same method was used to obtain complementary strains $\Delta adpA$::$adpA_{C62S}$, $\Delta adpA$::$adpA_{C126S}$, $\Delta adpA$::$adpA_{C187S}$, and $\Delta adpA$::$adpA_{C307S}$. The primers used in this process are shown in Table S2.

AdpA protein overexpression, purification, and mutation. To construct the AdpA expression strain, the coding sequence of $adpA$ was amplified from WT genomic DNA with the primers ExadpA-F/R. The PCR product was purified and ligated into the pET15b vector with a C-terminal His tag to create plasmid pET-AdpA by using the ClonExpress II one-step cloning kit (TaKaRa). The plasmid was transformed into *E. coli* BL21(DE3) cells, which were grown in LB medium at 37°C to an optical density at 600 nm (OD_{600}) of 0.6, and then a total of 0.5 mM isopropyl β-D-1-thiogalactopyranoside (IPTG) was added and an additional overnight cultivation was continued at 16°C. Cultures were collected by centrifugation and disrupted though a pressure cell homogenizer (SPCH-18) in sonication buffer (50 mM NaH_2PO_4, 250 mM NaCl, 20 mM imidazole, pH 8.0); 1 mM DTT was added before breaking the cells. Purification of the AdpA His-tagged proteins was performed with a Ni-NTA-Sefinose column (Sangon) as described previously (24). The protein purification process was conducted in an anaerobic glove box, which was filled with mixed gas (N_2, 85%; H_2, 10%; CO_2, 5%). The purity of the protein was assessed by SDS-PAGE gel, and its concentration was determined using the bicinchoninic acid (BCA) protein assay reagent (Thermo Fisher Scientific). The same method was used for purification of AdpA mutants.

Electrophoretic mobility shift assay (EMSA). The DNA probes containing AdpA binding sequences were amplified from genomic DNA. Different sulfane sulfur compounds were reacted with purified AdpA (and its mutants) in the binding buffer (20 mM Tris-HCl, 2 mM EDTA, 20 mM KCl, 0.5 mM dithiothreitol [DTT], pH 8.0) at room temperature for 20 min. Then DNA probe was added, and the binding reaction was performed at 30°C for 20 min. The binding complexes were separated on an 8% nondenaturing polyacrylamide gel at 120 V for 2 h in ice (58). The gel was dyed with SYBR green I (Sangon) for 20 min (44). All images were captured with a FluorChemQ system (Alpha Innotech).

RNA preparation, RT-PCR, and RT-qPCR. To extract RNA, spores (2×10^7) of WT and $\Delta adpA$ strains were inoculated into the liquid YBP medium and incubated at 30°C with shaking (220 rpm) for 36 h to the mid-exponential phase. HS_nH (400 μM) or S_8 (400 μM) was added. After another 30-min cultivation, these mycelia were harvested and ground into powder with liquid nitrogen. Similarly, the cultures of WT, $\Delta adpA$, and Δpdo were collected at the indicated times. All RNAs were isolated with a SteadyPure universal RNA extraction kit (Accurate Biology) following the manufacturer's instructions, and their quality and concentration were determined using a NanoDrop ND-1000 device (Thermo Fisher). RT-PCR was carried out using a reverse transcriptase kit (Invitrogen) and SYBR premix *Ex Taq* (TaKaRa) following the manufacturers' recommendations. The Roche LightCycler 480 thermal cycler was used (59). The expression of $hrdB$ mRNA was used as the internal standard to normalize the relative quantities of cDNA. The relative expression abundance of the target gene was analyzed using a relative quantification method ($2^{\Delta CT}$, test gene-$hrdB$). Three independent replicates were performed.

Phenotypic analysis and ACT production assay. *S. coelicolor* strains were cultured on solid YBP medium at 30°C for phenotypic analysis. ACT production was determined following a previously reported method (24, 60, 61). Briefly, *Streptomyces* strains were incubated on YBP medium for 7 or 10 days, and mycelia were harvested from the plate. KOH (1 M final concentration) was added to treat the mycelia for 4 h. Then the mixtures were centrifuged. The ACT concentration in the supernatant was determined by a spectrophotometer. Three independent biological experiments were replicated.

Construction and testing of EGFP reporter systems. To construct the reporter plasmids, promoter fragments (-400 to -1 upstream of *actII-4* and -460 to -1 upstream of *wblA*) were amplified using primers pMS82-*actII-4*p-*egfp* S1-F/R and pMS82-*wblA*p-*egfp* S1-F/R (Table S2). Then these promoter fragments and a DNA fragment encompassing the *egfp* gene were cloned into the pMS82 vector to generate pMS82-*actII-4*p-*egfp* and pMS82-*wblA*p-*egfp*. Next, we introduced these reporter plasmids into the WT and $\Delta adpA$.

Strains containing reporter plasmids were precultured in liquid YBP medium for 36 h at 30°C. Subsequently, equal amounts mycelia of each strain were transferred to the fluted bottle, and inducer (400 μM HS_nH or 400 μM S_8) was added. After 60 min of induction, the bacteria were collected by centrifugation, and mycelia were resuspended in 200 μL phosphate-buffered saline (PBS) buffer (OD_{450}, 2). EGFP fluorescence was measured using the microplate reader Synergy H1. The excitation wavelength and emission wavelength were set to 485 nm and 515 nm, respectively. The EGFP fluorescence intensity was normalized against cell density (fluorescence/OD_{450} of mycelia).

LC-MS/MS analysis of AdpA. The analysis was performed following a previous report (24). Freshly purified protein AdpA (<100 μg) was treated with 10-fold amounts of HS_nH (200 μM) or DTT (200 μM). After reacting at room temperature for 40 min. The reacted protein was treated with denaturing buffer (0.5 M Tris-HCl, 2.75 mM EDTA, 6 M guanidine-HCl, pH 8.0) containing 1 M iodoacetamide (IAM). The treatment was carried out in the dark for 1 h, and then the sample was digested with trypsin (1:25, wt/wt) at 37°C for 20 h. The digestion products were filtered by C_{18} Zip-Tip (Millipore) and vacuum-dried. The obtained peptides were resuspended in 10 μL double-distilled water (ddH$_2$O).

The Prominence nano-LC system (Shimadzu) equipped with a custom-made silica column (75 μm by 15 cm) packed with 3 μm ReproSil-Pur 120 C_{18}-AQ was used. Positive electrospray ionization was performed, and the ions were scanned with an LTQ-Orbitrap Velos Pro CID mass spectrometer (Thermo Scientific); the data were analyzed using a data-dependent acquisition mode with Xcalibur 2.2.0 software (Thermo Scientific). Full-scan MS spectra (from 400 to 1,800 *m/z*) were detected and assessed with the Orbitrap at a resolution of 60,000 at 400 *m/z*.

AdpA structure modeling. The AlphaFold 2 algorithm (62) was used to predict the tertiary structure of AdpA. This method used the custom multiple sequence alignment (MSA) option and was accessed via the Colab server on GitHub (https://github.com/sokrypton/ColabFold). The structural model of AdpA was analyzed and visualized with PyMOL.

Fluorescence polarization (FP) analysis. FP analysis experiments were performed following a reported protocol (63). DNA probes were amplified by PCR and labeled by 5′6-FAM (carboxyfluorescein) (Sangon). Purified AdpA (treated with 1 mM HS$_n$H for 10 min or not) was diluted to different concentrations (0.01 μM to ~22.5 μM). The reaction buffer contained 10 mM Tris–HCl and 75 mM NaCl, pH 7.5. After mixing diluted AdpA and labeled DNA in the reaction buffer, the solution was incubated at 37°C for 15 min in the dark. The fluorescence was detected with a BioTek Synergy HT instrument. The K_D value was calculated using GraphPad Prism 5 software.

SUPPLEMENTAL MATERIAL

Supplemental material is available online only.

TEXT S1, PDF file, 0.3 MB.
FIG S1, PDF file, 0.4 MB.
FIG S2, PDF file, 0.4 MB.
FIG S3, PDF file, 0.4 MB.
FIG S4, PDF file, 0.3 MB.
FIG S5, PDF file, 1.4 MB.
TABLE S1, PDF file, 0.3 MB.
TABLE S2, PDF file, 0.2 MB.

ACKNOWLEDGMENTS

REFERENCES

1. Sanchez J, Yague P, Manteca A. 2012. New insights in *Streptomyces* fermentations. Ferment Technol 1:e105. https://doi.org/10.4172/2167-7972.1000e105.

2. Olmos E, Mehmood N, Husein LH, Goergen JL, Fick M, Delaunay S. 2013. Effects of bioreactor hydrodynamics on the physiology of *Streptomyces*. Bioprocess Biosyst Eng 36:259–272. https://doi.org/10.1007/s00449-012-0794-1.

3. Hasani A, Kariminik A, Issazadeh K. 2014. *Streptomycetes*: characteristics and their antimicrobial activities. Int J Adv Biol Biomed Res 2:63–75.

4. Lee N, Hwang S, Kim J, Cho S, Palsson B, Cho BK. 2020. Mini review: genome mining approaches for the identification of secondary metabolite biosynthetic gene clusters in *Streptomyces*. Comput Struct Biotechnol J 18:1548–1556. https://doi.org/10.1016/j.csbj.2020.06.024.

5. Honma S, Ito S, Yajima S, Sasaki Y. 2021. Nitric oxide signaling for actinorhodin production in *Streptomyces coelicolor* A3(2) via the DevS/R two-component system. Appl Environ Microbiol 87:e00480-21. https://doi.org/10.1128/AEM.00480-21.

6. Lee N, Hwang S, Kim W, Lee Y, Kim JH, Cho S, Kim HU, Yoon YJ, Oh MK, Palsson BO, Cho BK. 2021. Systems and synthetic biology to elucidate secondary metabolite biosynthetic gene clusters encoded in *Streptomyces* genomes. Nat Prod Rep 38:1330–1361. https://doi.org/10.1039/d0np00071j.

7. Ohnishi Y, Yamazaki H, Kato JY, Tomono A, Horinouchi S. 2005. AdpA, a central transcriptional regulator in the A-factor regulatory cascade that leads to morphological development and secondary metabolism in *Streptomyces griseus*. Biosci Biotechnol Biochem 69:431–439. https://doi.org/10.1271/bbb.69.431.

8. den Hengst CD, Tran NT, Bibb MJ, Chandra G, Leskiw BK, Buttner MJ. 2010. Genes essential for morphological development and antibiotic production in *Streptomyces coelicolor* are targets of BldD during vegetative growth. Mol Microbiol 78:361–379. https://doi.org/10.1111/j.1365-2958.2010.07338.x.

9. Yan H, Lu XR, Sun D, Zhuang S, Chen Q, Chen Z, Li JL, Wen Y. 2020. BldD, a master developmental repressor, activates antibiotic production in two *Streptomyces* species. Mol Microbiol 113:123–142. https://doi.org/10.1111/mmi.14405.

10. Setinova D, Smidova K, Pohl P, Music I, Bobek J. 2017. RNase III-binding-mRNAs revealed novel complementary transcripts in *Streptomyces*. Front Microbiol 8:2693. https://doi.org/10.3389/fmicb.2017.02693.

11. Takano E, Tao M, Long F, Bibb MJ, Wang L, Li W, Buttner MJ, Bibb MJ, Deng ZX, Chater KF. 2003. A rare leucine codon in *adpA* is implicated in the morphological defect of *bldA* mutants of *Streptomyces coelicolor*. Mol Microbiol 50:475–486. https://doi.org/10.1046/j.1365-2958.2003.03728.x.

12. Koshla O, Yushchuk O, Stash I, Dacyuk Y, Myronovskyi M, Jager G, Sussmuth RD, Luzhetskyy A, Bystrom A, Kirsebom LA, Ostash B. 2019. Gene *miaA* for post-transcriptional modification of tRNA$_{XXA}$ is important for morphological and metabolic differentiation in *Streptomyces*. Mol Microbiol 112:249–265. https://doi.org/10.1111/mmi.14266.

13. Kato J, Ohnish Y, Horinouchi S. 2005. Autorepression of AdpA of the AraC/XylS family, a key transcriptional activator in the A-factor regulatory cascade in *Streptomyces griseus*. J Mol Biol 350:12–26. https://doi.org/10.1016/j.jmb.2005.04.058.

14. Rabyk M, Yushchuk O, Rokytskyy I, Anisimova M, Ostash B. 2018. Genomic insights into evolution of AdpA family master regulators of morphological differentiation and secondary metabolism in *Streptomyces*. J Mol Evol 86:204–215. https://doi.org/10.1007/s00239-018-9834-z.

15. Lau N, Pluth MD. 2019. Reactive sulfur species (RSS): persulfides, polysulfides, potential, and problems. Curr Opin Chem Biol 49:1–8. https://doi.org/10.1016/j.cbpa.2018.08.012.

16. Filipovic MR, Zivanovic J, Alvarez B, Banerjee R. 2018. Chemical biology of H$_2$S signaling through persulfidation. Chem Rev 118:377–461. https://doi.org/10.1021/acs.chemrev.7b00205.

17. Fukuto JM, Ignarro LJ, Nagy P, Wink DA, Kevil CG, Feelisch M, Cortese-Krott MM, Bianco CL, Kumagai Y, Hobbs AJ, Lin J, Ida T, Akaike T. 2018. Biological hydropersulfides and related polysulfides: a new concept and perspective in redox biology. FEBS Lett 592:2140–2152. https://doi.org/10.1002/1873-3468.13090.

18. Toohey JI, Cooper AJL. 2014. Thiosulfoxide (sulfane) sulfur: new chemistry and new regulatory roles in biology. Molecules 19:12789–12813. https://doi.org/10.3390/molecules190812789.

19. Wang SSS, Chen YHH, Chen N, Wang LJJ, Chen DXX, Weng HLL, Dooley S, Ding HGG. 2017. Hydrogen sulfide promotes autophagy of hepatocellular carcinoma cells through the PI3K/Akt/mTOR signaling pathway. Cell Death Dis 8:e2688. https://doi.org/10.1038/cddis.2017.18.

20. Xin YF, Gao R, Cui FF, Lü CJ, Liu HL, Liu HW, Xia YZ, Xun LY. 2020. The heterotrophic bacterium *Cupriavidus pinatubonensis* JMP134 oxidizes sulfide

to sulfate with thiosulfate as a key intermediate. Appl Environ Microbiol 86:e01835-20. https://doi.org/10.1128/AEM.01835-20.

21. Wunder LC, Aromokeye DA, Yin XR, Richter-Heitmann T, Willis-Poratti G, Schnakenberg A, Otersen C, Dohrmann I, Romer M, Bohrmann G, Kasten S, Friedrich MW. 2021. Iron and sulfate reduction structure microbial communities in (sub-)Antarctic sediments. ISME J 15:3587–3604. https://doi.org/10.1038/s41396-021-01014-9.

22. Peng H, Zhang YX, Palmer LD, Kehl-Fie TE, Skaar EP, Trinidad JC, Giedroc DP. 2017. Hydrogen sulfide and reactive sulfur species impact proteome S-sulfhydration and global virulence regulation in Staphylococcus aureus. ACS Infect Dis 3:744–755. https://doi.org/10.1021/acsinfecdis.7b00090.

23. Liu DX, Zhang JJ, Lü CJ, Xia YZ, Liu HW, Jiao NZ, Xun LY, Liu JH. 2020. Synechococcus sp. strain PCC7002 uses sulfide:quinone oxidoreductase to detoxify exogenous sulfide and to convert endogenous sulfide to cellular sulfane sulfur. mBio 11:e03420-19. https://doi.org/10.1128/mBio.03420-19.

24. Lu T, Cao Q, Pang XH, Xia YZ, Xun LY, Liu HW. 2020. Sulfane sulfur-activated actinorhodin production and sporulation is maintained by a natural gene circuit in Streptomyces coelicolor. Microb Biotechnol 13:1917–1932. https://doi.org/10.1111/1751-7915.13637.

25. Park SS, Yang YH, Song E, Kim EJ, Kim WS, Sohng JK, Lee HC, Liou KK, Kim BG. 2009. Mass spectrometric screening of transcriptional regulators involved in antibiotic biosynthesis in Streptomyces coelicolor A3(2). J Ind Microbiol Biotechnol 36:1073–1083. https://doi.org/10.1007/s10295-009-0591-2.

26. Liu G, Chater KF, Chandra G, Niu GQ, Tan HR. 2013. Molecular regulation of antibiotic biosynthesis in Streptomyces. Microbiol Mol Biol Rev 77:112–143. https://doi.org/10.1128/MMBR.00054-12.

27. Kimura Y, Koike S, Shibuya N, Lefer D, Ogasawara Y, Kimura H. 2017. 3-Mercaptopyruvate sulfurtransferase produces potential redox regulators cysteine- and glutathione-persulfide (Cys-SSH and GSSH) together with signaling molecules H_2S_2, H_2S_3 and H_2S. Sci Rep 7:10459. https://doi.org/10.1038/s41598-017-11004-7.

28. Arias P, Fernandez-Moreno MA, Malpartida F. 1999. Characterization of the pathway-specific positive transcriptional regulator for actinorhodin biosynthesis in Streptomyces coelicolor A3(2) as a DNA-binding protein. J Bacteriol 181:6958–6968. https://doi.org/10.1128/JB.181.22.6958-6968.1999.

29. Lee HN, Kim JS, Kim P, Lee HS, Kim ES. 2013. Repression of antibiotic downregulator WblA by AdpA in Streptomyces coelicolor. Appl Environ Microbiol 79:4159–4163. https://doi.org/10.1128/AEM.00546-13.

30. Wolanski M, Donczew R, Kois-Ostrowska A, Masiewicz P, Jakimowicz D, Zakrzewska-Czerwinska J. 2011. The level of AdpA directly affects expression of developmental genes in Streptomyces coelicolor. J Bacteriol 193:6358–6365. https://doi.org/10.1128/JB.05734-11.

31. Mustafa AK, Gadalla MM, Sen N, Kim S, Mu WT, Gazi SK, Barrow RK, Yang GD, Wang R, Snyder SH. 2009. H_2S signals through protein S-sulfhydration. Sci Signal 2:ra72.

32. Paul BD, Snyder SH. 2015. Protein sulfhydration. Methods Enzymol 555:79–90. https://doi.org/10.1016/bs.mie.2014.11.021.

33. Bu XL, Weng JY, He BB, Xu MJ, Xu J. 2019. A novel AdpA homologue negatively regulates morphological differentiation in Streptomyces xiamenensis 318. Appl Environ Microbiol 85:e03107-18. https://doi.org/10.1128/AEM.03107-18.

34. Kang YJ, Wang YY, Hou BB, Wang RD, Ye J, Zhu XY, Wu HZ, Zhang HZ. 2019. AdpA$_{lin}$, a pleiotropic transcriptional regulator, is involved in the cascade regulation of lincomycin biosynthesis in Streptomyces lincolnensis. Front Microbiol 10:2428. https://doi.org/10.3389/fmicb.2019.02428.

35. Yushchuk O, Ostash I, Vlasiuk I, Gren T, Luzhetskyy A, Kalinowski J, Fedorenko V, Ostash B. 2018. Heterologous AdpA transcription factors enhance landomycin production in Streptomyces cyanogenus S136 under a broad range of growth conditions. Appl Microbiol Biotechnol 102:8419–8428. https://doi.org/10.1007/s00253-018-9249-1.

36. Xu JJ, Zhang JH, Zhuo JM, Li Y, Tian YQ, Tan HR. 2017. Activation and mechanism of a cryptic oviedomycin gene cluster via the disruption of a global regulatory gene, adpA, in Streptomyces ansochromogenes. J Biol Chem 292:19708–19720. https://doi.org/10.1074/jbc.M117.809145.

37. Mao XM, Luo S, Zhou RC, Wang F, Yu P, Sun N, Chen XX, Tang Y, Li YQ. 2015. Transcriptional regulation of the daptomycin gene cluster in Streptomyces roseosporus by an autoregulator, AtrA. J Biol Chem 290:7992–8001. https://doi.org/10.1074/jbc.M114.608273.

38. Zacharia VM, Ra Y, Sue C, Alcala E, Reaso JN, Ruzin SE, Traxler MF. 2021. Genetic network architecture and environmental cues drive spatial organization of phenotypic division of labor in Streptomyces coelicolor. mBio 12:e00794-21. https://doi.org/10.1128/mBio.00794-21.

39. Ran MX, Wang TQ, Shao M, Chen ZG, Liu HW, Xia YZ, Xun LY. 2019. Sensitive method for reliable quantification of sulfane sulfur in

biological samples. Anal Chem 91:11981–11986. https://doi.org/10.1021/acs.analchem.9b02875.

40. Hou NK, Yan ZZ, Fan KL, Li HJ, Zhao R, Xia YZ, Xun LY, Liu HW. 2019. OxyR senses sulfane sulfur and activates the genes for its removal in Escherichia coli. Redox Biol 26:101293. https://doi.org/10.1016/j.redox.2019.101293.

41. Fan KL, Chen ZG, Liu HW. 2020. Evidence that the ProPerDP method is inadequate for protein persulfidation detection due to lack of specificity. Sci Adv 6:eabb6477. https://doi.org/10.1126/sciadv.abb6477.

42. de Lira NPV, Pauletti BA, Marques AC, Perez CA, Caserta R, de Souza AA, Vercesi AE, Leme AFP, Benedetti CE. 2018. BigR is a sulfide sensor that regulates a sulfur transferase/dioxygenase required for aerobic respiration of plant bacteria under sulfide stress. Sci Rep 8:3508. https://doi.org/10.1038/s41598-018-21974-x.

43. Luebke JL, Shen JC, Bruce KE, Kehl-Fie TE, Peng H, Skaar EP, Giedroc DP. 2014. The CsoR-like sulfurtransferase repressor (CstR) is a persulfide sensor in Staphylococcus aureus. Mol Microbiol 94:1343–1360. https://doi.org/10.1111/mmi.12835.

44. Li HJ, Li J, Lü CJ, Xia YZ, Xin YF, Liu HL, Xun LY, Liu HW. 2017. FisR activates σ^{54}-dependent transcription of sulfide-oxidizing genes in Cupriavidus pinatubonensis JMP134. Mol Microbiol 105:373–384. https://doi.org/10.1111/mmi.13725.

45. Shimizu T, Shen JC, Fang MX, Zhang YX, Hori K, Trinidad JC, Bauer CE, Giedroc DP, Masuda S. 2017. Sulfide-responsive transcriptional repressor SqrR functions as a master regulator of sulfide-dependent photosynthesis. Proc Natl Acad Sci U S A 114:2355–2360. https://doi.org/10.1073/pnas.1614133114.

46. Capdevila DA, Walsh BJC, Zhang YF, Dietrich C, Gonzalez-Gutierrez G, Giedroc DP. 2021. Structural basis for persulfide-sensing specificity in a transcriptional regulator. Nat Chem Biol 17:65–70. https://doi.org/10.1038/s41589-020-00671-9.

47. Giedroc DP. 2017. A new player in bacterial sulfide-inducible transcriptional regulation. Mol Microbiol 105:347–352. https://doi.org/10.1111/mmi.13726.

48. Xuan GH, Lü CJ, Xu HW, Chen ZG, Li K, Liu HL, Liu HW, Xia YZ, Xun LY. 2020. Sulfane sulfur is an intrinsic signal activating MexR-regulated antibiotic resistance in Pseudomonas aeruginosa. Mol Microbiol 114:1038–1048. https://doi.org/10.1111/mmi.14593.

49. Kieser T, Bibb MJ, Buttner MJ, Chater KF, Hopwood DA. 2000. Practical Streptomyces genetics, 2nd ed. John Innes Foundation, Norwich, UK.

50. Zhu YP, Lu T, Zhang J, Zhang PP, Tao MF, Pang XH. 2020. A novel XRE family regulator that controls antibiotic production and development in Streptomyces coelicolor. Appl Microbiol Biotechnol 104:10075–10089. https://doi.org/10.1007/s00253-020-10950-z.

51. Visser JM, Robertson LA, Van Verseveld HW, Kuenen JG. 1997. Sulfur production by obligately chemolithoautotrophic Thiobacillus species. Appl Environ Microbiol 63:2300–2305. https://doi.org/10.1128/aem.63.6.2300-2305.1997.

52. Xin YF, Liu HL, Cui FF, Liu HW, Xun LY. 2016. Recombinant Escherichia coli with sulfide:quinone oxidoreductase and persulfide dioxygenase rapidly oxidises sulfide to sulfite and thiosulfate via a new pathway. Environ Microbiol 18:5123–5136. https://doi.org/10.1111/1462-2920.13511.

53. Flavin M. 1962. Microbial transsulfuration: the mechanism of an enzymatic disulfide elimination reaction. J Biol Chem 237:768–777. https://doi.org/10.1016/S0021-9258(18)60371-0.

54. Lu T, Zhu YP, Zhang PP, Sheng DH, Cao GX, Pang XH. 2018. SCO5351 is a pleiotropic factor that impacts secondary metabolism and morphological development in Streptomyces coelicolor. FEMS Microbiol Lett 365:fny150. https://doi.org/10.1093/femsle/fny150.

55. Zhu YP, Xu WH, Zhang J, Zhang PP, Zhao ZL, Sheng DH, Ma W, Zhang YZ, Bai LQ, Pang XH. 2020. A hierarchical network of four regulatory genes controlling production of the polyene antibiotic candicidin in Streptomyces sp. strain FR-008. Appl Environ Microbiol 86:e00055-20. https://doi.org/10.1128/AEM.00055-20.

56. Gregory MA, Till R, Smith MCM. 2003. Integration site for Streptomyces phage phiBT1 and development of site-specific integrating vectors. J Bacteriol 185:5320–5323. https://doi.org/10.1128/JB.185.17.5320-5323.2003.

57. Xia YZ, Chu WQ, Qi QS, Xun LY. 2015. New insights into the QuikChange™ process guide the use of Phusion DNA polymerase for site-directed mutagenesis. Nucleic Acids Res 43:e12. https://doi.org/10.1093/nar/gku1189.

58. Zhu YP, Zhang PP, Zhang J, Xu WH, Wang XY, Wu LL, Sheng DH, Ma W, Cao GX, Chen XA, Lu YH, Zhang YZ, Pang XH. 2019. The developmental regulator MtrA binds GlnR boxes and represses nitrogen metabolism genes in Streptomyces coelicolor. Mol Microbiol 112:29–46. https://doi.org/10.1111/mmi.14252.

59. Zhu YP, Zhang PP, Lu T, Wang XY, Li AY, Lu YH, Tao MF, Pang XH. 2021. Impact of MtrA on phosphate metabolism genes and the response to altered phosphate conditions in *Streptomyces*. Environ Microbiol 23: 6907–6923. https://doi.org/10.1111/1462-2920.15719.

60. Liu M, Zhang PP, Zhu YP, Lu T, Wang YM, Cao GX, Shi M, Chen XL, Tao MF, Pang XH. 2019. Novel two-component system MacRS is a pleiotropic regulator that controls multiple morphogenic membrane protein genes in *Streptomyces coelicolor*. Appl Environ Microbiol 85:e02178-18. https://doi.org/10.1128/AEM.02178-18.

61. Zhu YP, Zhang PP, Zhang J, Wang J, Lu YH, Pang XH. 2020. Impact on multiple antibiotic pathways reveals MtrA as a master regulator of antibiotic production in *Streptomyces* spp. and potentially in other actinobacteria. Appl Environ Microbiol 86:e01201-20. https://doi.org/10.1128/AEM.01201-20.

62. Jumper J, Evans R, Pritzel A, Green T, Figurnov M, Ronneberger O, Tunyasuvunakool K, Bates R, Zidek A, Potapenko A, Bridgland A, Meyer C, Kohl SAA, Ballard AJ, Cowie A, Romera-Paredes B, Nikolov S, Jain R, Adler J, Back T, Petersen S, Reiman D, Clancy E, Zielinski M, Steinegger M, Pacholska M, Berghammer T, Bodenstein S, Silver D, Vinyals O, Senior AW, Kavukcuoglu K, Kohli P, Hassabis D. 2021. Highly accurate protein structure prediction with AlphaFold. Nature 596:583–589. https://doi.org/10.1038/s41586-021-03819-2.

63. Zhang FY, Li BQ, Dong HJ, Chen M, Yao S, Li JW, Zhang HH, Liu XG, Wang HW, Song NN, Zhang KD, Du N, Xu SJ, Gu LC. 2020. YdiV regulates *Escherichia coli* ferric uptake by manipulating the DNA-binding ability of Fur in a SlyD-dependent manner. Nucleic Acids Res 48:9571–9588. https://doi.org/10.1093/nar/gkaa696.